Coupled Antiferromagnetic–Nuclear-Magnetic Resonance in RbMnF₃†

W. J. INCE*

*Department of Electrical Engineering and Center for Materials Science and Engineering,
Massachusetts Institute of Technology, Cambridge, Massachusetts 02139*

(Received 13 March 1969)

The coupling between antiferromagnetic and Mn^{55} nuclear resonances in RbMnF₃ has been studied both theoretically and experimentally. The electronic and nuclear frequencies have been derived by solving the coupled equations of motion for (a) a four-sublattice model, consisting of two electronic and two nuclear magnetic sublattices; (b) a two-sublattice model in which the electron-nuclear interaction is represented by a static anisotropy field. For the electronic modes, the differences in the frequencies obtained from the two models are negligible. However, only the four-sublattice theory predicts the NMR frequencies to good accuracy, for applied fields both greater and less than the spin-flop value. The temperature dependence of the crystal parameters has been included, and comparison is made between theory and experiment in the temperature range where the parallel susceptibility is significant.

I. INTRODUCTION

WITHIN the last few years, the group of compounds $X\,MnF_3$, where X is Rb, K, or Cs, has been the subject of extensive investigations.[1] These materials, which have the perovskite structure (with the exception of CsMnF₃), are antiferromagnetic below their Néel temperatures of 82.6, 88.3, and 53.5°K respectively. The combination of large effective exchange field ($\sim 10^6$ Oe) and small anisotropy (< 10 Oe) permit AFMR to be observed conveniently at X-band frequencies without the necessity of large magnetizing fields. Another interesting feature is the large nuclear hyperfine interaction which, because of the small crystalline anisotropy, causes the nuclear and antiferromagnetic resonance modes to be strongly coupled. The resonant frequencies are considerably shifted by the perturbation. It also gives rise to a temperature dependence of the AFMR frequencies at low temperatures and greatly enhances the intensity of the nuclear modes. Consequently, magnetic resonance has proved to be a valuable means for studying the hyperfine interaction in such materials.

This paper is devoted to a study of magnetic resonance in RbMnF₃. Of the above trio of compounds, RbMnF₃ has the simplest antiferromagnetic configuration. It appears to remain cubic down to the lowest temperatures.[2] The Mn^{2+} ions form a two-sublattic antiparallel arrangement of electronic spins, the $\langle 111 \rangle$ axes being the easy directions of magnetization. In contrast, KMnF₃ undergoes a second transition at 81.5°K into a canted configuration which results in a small net moment.[3] Uniaxial, orthorhombic, and cubic terms have been used to characterize the crystalline anisotropy

energy.[4] As a result of the distortion, there are two inequivalent Mn^{2+} sites, so that the electron spins can be described by a four-sublattice configuration.

CsMnF₃ has a hexagonal arrangement.[5] The anisotropy in the basal plane, which is an easy plane, is negligible. The most recent theoretical treatments[6,7] of the resonance behavior of both KMnF₃ and CsMnF₃ have used a model comprising four electronic sublattices, which predicts a total of four AFMR modes. Two of these are high-frequency exchange modes, the remaining two being low-frequency modes.

The simple cubic structure of RbMnF₃ makes it attractive for both theoretical and experimental investigations. For example, the temperature dependence of the sublattice magnetization has been recently determined[8] from measurement of the Mn^{55} NMR frequency as a function of temperature. Spin-wave theory[9] predicts a T^2 dependence of sublattice magnetization for antiferromagnets at low temperatures, whereas the observed variation is more nearly cubic. Similar information has been obtained[10] from measurements of the variation of the anisotropy constant with temperature.

The AFMR properties of RbMnF₃ were first reported by Teaney et al.,[2] who calculated values of 4.47 Oe and 8.9×10^5 Oe for the anisotropy and exchange fields, respectively, from resonance data. The strong temperature dependence of the AFMR frequencies was noted. Heeger et al.[3,11] had previously noted similar effects in KMnF₃, which were correctly attributed to the hyperfine interaction. Teaney et al.[2] included an effective field, acting on the electrons, due to the polarization of the paramagnetic nuclear moments. The magnitude of this field, which at low temperatures is equal to $9.43°K/T$ Oe for RbMnF₃, was deduced from EPR measurements[12] of Mn^{55} in diamagnetic KMgF₃.

---

[1] For an extensive bibliography relating to these compounds, see J. S. Friebely and W. J. Ince, M.I.T. Lincoln Laboratory Library, 33rd Ref. Bibliography, 1968.
[2] D. T. Teaney et al., Phys. Rev. Letters 9, 212 (1962).
[3] A. J. Heeger et al., Phys. Rev. 123, 1652 (1961).

[4] A. M. Portis et al., J. Appl. Phys. 34, 1052 (1963).
[5] K. Lee et al., Phys. Rev. 132, 144 (1963).
[6] V. Minkiewicz and A. Nakamura, Phys. Rev. 143, 356 (1966).
[7] L. B. Welsh, Phys. Rev. 156, 370 (1967).
[8] D. T. Teaney, Bull. Am. Phys. Soc. 13, 164 (1968).
[9] T. Oguchi, Phys. Rev. 117, 117 (1960).
[10] P. E. Seiden, Phys. Letters 28A, 239 (1968).
[11] A. J. Heeger et al., Phys. Rev. Letters 7, 307 (1961).
[12] H. Montgomery et al., Phys. Rev. 128, 80 (1961).

In much of the early resonance work on RbMnF₃, use was made of the flopped configuration,[2,13–16] i.e., the applied field was large enough to ensure that the magnetization was almost perpendicular to the field direction. For small values of applied field, the magnetization is not, in general, flopped. The mode spectra are more complex and the resonance analysis is more difficult. This region was investigated by Ince.[17,18] Calculation of the resonant frequencies required a knowledge of the static equilibrium position of the magnetization with respect to the applied field and the crystal axes. This was obtained for the case of the magnetization lying in a 110 plane. With improvements to the analysis, Cole and Ince[19] obtained close agreement between the calculated and experimentally observed AFMR spectra over a wide range of applied field. When the magnetization is flopped, one of the two AFMR modes is field independent. This mode was first observed by Freiser, et al.[14]

The AFMR linewidth has been shown[20] to be inhomogeneously broadened. For the samples used in the present work, $2\Delta H$ ranged roughly between 90 and 300 Oe at 4.2°K, compared with 175 Oe reported by Eastman.[20] From pressure-dependent AFMR experiments, he estimated the intrinsic linewidth to be less than 5 Oe.

NMR of Mn⁵⁵ in RbMnF₃ was first reported by Heeger and Teaney.[15] They showed that the NMR signal in the flopped configuration was sufficiently enhanced by the hyperfine interaction for the resonance to be observed, using only dc detection. Subsequent investigations,[16] using an experimental arrangement having higher resolution, have revealed the existence of a mode splitting which occurs in an applied field strength of about 13 kOe. No explanation of this effect has yet been put forward.

Since the effective field at the Mn⁵⁵ nucleus is of the order of 10⁵ Oe, the NMR frequencies lie in the uhf region of the spectrum. Theoretically, two nuclear modes should exist, but observation of only one of the mode branches has been reported previously. In Sec. IV, experimental verification of both nuclear modes is reported.

In magnetically ordered materials, the nuclear spins are indirectly coupled via the Suhl-Nakamura (S-N) interaction.[21,22] Estimates of the nuclear linewidth, based upon the S-N interaction, are an order of magnitude greater than the observed linewidth. The latter is

approximately 100 Oe ($\approx$ 100 kHz) in RbMnF₃ for the spin-flop configuration. Richards[23] has recently shown that if a well-defined nuclear spin-wave spectrum exists, the estimated linewidth is much less than the second moment of the S-N interaction. However, his estimate is two orders of magnitude *less* than the experimental width. Richard's value is reconciled with the observed value if the influence of random strains is taken into account.

In most of the previous work dealing with AFMR in materials which possess a strong nuclear hyperfine interaction, a common assumption has been made. Namely, the nuclei cannot react instantaneously to the precession of the electronic spins. The effect of the hyperfine interaction on the electrons has been represented by a static field, pointing in the direction of the sublattice magnetization. Conversely, the response of the electronic spins to the nuclear precession is assumed adiabatic, i.e., they can follow the motion of the nuclei without delay.

The degree of error introduced by the above approximations, which is likely to be greatest at low temperatures ($\approx$ 1°K), has been investigated for the case of RbMnF₃. The equations of motion have been solved in a self-consistent manner, taking into account the instantaneous correlation between the electronic and nuclear spins. The model for this analysis comprises four magnetic sublattices—two electronic and two nuclear. The temperature dependence of the normal mode frequencies, based upon molecular field approximations, has also been calculated.

In the following, we shall first discuss the terms which comprise the Hamiltonian of the free energy. The problem of determining the orientation of the magnetic sublattices under the action of an applied field will then be considered. Next, the resonance analysis, based on a two-sublattice model, is reviewed. In Sec. V, the four-sublattice model is introduced, in order to account for the dynamic electron-nuclear interaction. The coupled equations of motion for two electronic and two nuclear sublattices are solved and the resulting characteristic frequencies of the system compared with those obtained using the simpler approach. Finally, experimental studies of the electronic and nuclear modes in RbMnF₃ are described and the data compared with the computed spectra.

II. HAMILTONIAN

Throughout this work, the semiclassical approach will be taken. It will be assumed that quantum mechanical angular momentum operators can be represented by classical vectors.[24] The ground-state energy can then be obtained by replacing spin or magnetization operators in the Hamiltonian by vector quantities.

[13] D. T. Teaney, Bull. Am. Phys. Soc. **7**, 201 (1962).
[14] M. J. Freiser *et al.*, Phys. Rev. Letters **10**, 293 (1963).
[15] A. J. Heeger and D. T. Teaney, J. Appl. Phys. **35**, 846 (1964).
[16] M. J. Freiser *et al.*, in *Proceedings of the International Conference on Magnetism, Nottingham, 1964* (Institute of Physics and The Physical Society, London, 1965), p. 432.
[17] W. J. Ince, S. M. thesis, M.I.T., 1965 (unpublished).
[18] W. J. Ince, J. Appl. Phys. **37**, 1122 (1966).
[19] P. H. Cole and W. J. Ince, Phys. Rev. **150**, 377 (1966).
[20] D. E. Eastman, Phys. Rev. **156**, 645 (1967).
[21] H. Suhl, Phys. Rev. **109**, 606 (1958).
[22] T. Nakamura, Progr. Theoret. Phys. (Kyoto) **20**, 542 (1958).

[23] P. M. Richards, Phys. Rev. **173**, 581 (1968).
[24] S. Tyablikov, *Methods in the Quantum Theory of Magnetism* (Plenum Press, Inc., New York, 1967).

The terms which will be considered in the free energy are exchange, anisotropy, Zeeman, and nuclear hyperfine interaction energies. $RbMnF_3$ has the cubic perovskite structure, the lattice constant being[25] (4.2396±0.0002)Å. The unit cell, whose dimension is equal to the lattice constant, contains a single Mn^{2+} ion located at the cube center, Rb^+ ions at the cube corners, and F^- ions at the centers of the cube faces. The divalent manganese ions are situated at octahedral sites, and the super-exchange mechanism, which acts via the F^- ions, is responsible for the antiferromagnetic alignment. The exchange term in the Hamiltonian of the free energy density can be represented by an isotropic interaction

$$\mathcal{H}_E = -\tfrac{1}{2}W_{11}(\mathbf{M}_1\cdot\mathbf{M}_1+\mathbf{M}_2\cdot\mathbf{M}_2)-W_{12}\mathbf{M}_1\cdot\mathbf{M}_2, \quad (1)$$

where $\mathbf{M}_1$ and $\mathbf{M}_2$ are the electronic sublattice magnetizations and W_{11} and W_{12} are the exchange constants.

The anisotropy energy for a material having cubic symmetry may be expressed as a power-series expansion of the direction cosines of the sublattice magnetization. The lowest term in the series is the only one needed to represent the anisotropy term for $RbMnF_3$:

$$\mathcal{H}_a = \sum_{i=1}^{2}\frac{K}{2M_i{}^4}(M_{ix}{}^2M_{iy}{}^2+M_{iy}{}^2M_{iz}{}^2+M_{iz}{}^2M_{ix}{}^2),$$
$$K<0, \quad i=1,2. \quad (2)$$

The Cartesian coordinate axes coincide with the crystal axes.

The magnetic interaction between a nucleus and the ionic electrons[26] is usually written as

$$\mathcal{H}_{hf} = -g_Eg_N\mu_E\mu_N(8\pi/3)\delta(\mathbf{r})\mathbf{S}\cdot\mathbf{I}$$
$$+[(\mathbf{L}-\mathbf{S})\cdot\mathbf{I}/r^3]+[3(\mathbf{S}\cdot\mathbf{r})(\mathbf{I}\cdot\mathbf{r})/r^5]. \quad (3)$$

Here, g_E and g_N are the electron and nuclear g factors, μ_E and μ_N the Bohr and nuclear magnetons, $\mathbf{L}$ and $\mathbf{S}$ are the usual electronic orbital and spin quantum numbers, and $\mathbf{I}$ is the nuclear spin quantum number. The vector $\mathbf{r}$ is the radius vector, measured from the nucleus. For the Mn^{2+} ion, there is no orbital angular momentum, i.e., $\mathbf{L}=0$.

In order to find the mean hyperfine interaction, Eq. (3) is integrated over all space. When this is done, the two terms, which are analogous to the classical dipolar interaction, average to zero for a spherically symmetrical ion. The first term in Eq. (3) is the so-called Fermi contact term, and is a measure of the overlap of the electronic charge cloud and the nucleus. If there are no unpaired s electrons, the Fermi contact term is generally zero. Hence, one might erroneously conclude that the hyperfine interaction is zero for the Mn^{2+} ion. The origin of the very large hyperfine interaction that is found experimentally for Mn^{2+} is generally

[25] C. G. Windsor and R. W. H. Stevenson, Proc. Phys. Soc. (London) **87**, 501 (1966).
[26] R. E. Watson and A. J. Freeman, Phys. Rev. **123**, 2027 (1961).

attributed[26] to a polarization of the core s electrons via the $3d$ electrons.

When $\mathbf{L}$ is zero, Eq. (3) can be rewritten in the form

$$\mathcal{H}_{hf}=A\mathbf{I}\cdot\mathbf{S}, \quad (4)$$

where A is the hyperfine constant. This energy may be considered to arise from an equivalent magnetic field, acting upon the nuclear moment, having an average value H_{NN}, given by

$$H_{NN}=A\langle S\rangle/\gamma\hbar, \quad (5)$$

γ being the nuclear gyromagnetic ratio. This field, in the case of $RbMnF_3$, has a value[15] of about 6.5×10^5 Oe at 4.2°K. For Mn^{2+} ions, H_{NN} is negative, i.e., the direction of the field is antiparallel to the net spin of the ion. However, since the nuclear and electronic gyromagnetic ratios have opposite sign, the corresponding moments are aligned. From the macroscopic viewpoint, the magnetization comprises four distinct sublattices—two electronic and two nuclear. The nuclear polarization produces an equivalent field H_{NE} acting on the electronic moments. The paramagnetic nature of the nuclear polarization is reflected by a temperature dependence which follows the Curie law. The average value of H_{NE} is

$$H_{NE}=\frac{A^2}{\Gamma\hbar}\frac{\langle S_z\rangle I(I+1)}{3kT}, \quad (6)$$

where Γ is the electronic gyromagnetic ratio. The physical significance of the two hyperfine fields becomes clear if we neglect for the moment all dynamic correlation between nuclear and electronic spins. H_{NE} is equivalent to an effective anisotropy field, since it is always aligned with the direction of the static magnetization. It simply gets added to the crystalline anisotropy field in the expressions for the AFMR frequencies. Hence, the hyperfine interaction raises the antiferromagnetic frequencies by approximately $\Gamma(2H_EH_{NE})^{1/2}$, where H_E is the exchange field.

In the absence of dynamic correlation, the nuclei would precess in the static field H_{NN} at a frequency equal to γH_{NN} which is approximately 686 MHz. By comparison, the effect of an externally applied field in the range 0–10 000 Oe would have negligible effect on the NMR frequencies beyond removing the degeneracy.

When the electron-nuclear correlation is included the nuclear frequencies are lowered or "pulled" from their unperturbed values. The frequency depression can be in excess of 100 MHz below the "unpulled" hyperfine frequency γH_{NN}.

The hyperfine interaction energy expressed by Eq. (4) can be put in a more convenient form, as a function of the electronic and nuclear sublattice magnetizations $\mathbf{M}_1$, $\mathbf{M}_2$, and $\mathbf{N}_1$, $\mathbf{N}_2$:

$$\mathcal{H}_{hf}=-\alpha(\mathbf{N}_1\cdot\mathbf{M}_1+\mathbf{N}_2\cdot\mathbf{M}_2),$$

where α is a coupling coefficient. The Hamiltonian $\mathcal{3C}$ for the four-sublattice system can now be written down:

$$\mathcal{3C}=\mathcal{3C}_{ex}+\mathcal{3C}_{an}+\mathcal{3C}_{Zeeman}+\mathcal{3C}_{hf}$$

$$=-\tfrac{1}{2}W_{11}(\mathbf{M}_1\cdot\mathbf{M}_1+\mathbf{M}_2\cdot\mathbf{M}_2)-W_{12}\mathbf{M}_1\cdot\mathbf{M}_2$$

$$+\sum_{i=1}^{2}\frac{K}{2M_i^4}(M_{ix}^2M_{iy}^2+M_{iy}^2M_{iz}^2+M_{iz}^2M_{ix}^2)$$

$$-(\mathbf{M}_1+\mathbf{M}_2)\cdot\mathbf{H}_0-(\mathbf{N}_1+\mathbf{N}_2)\cdot\mathbf{H}_0$$

$$-\alpha(\mathbf{N}_1\cdot\mathbf{M}_1+\mathbf{N}_2\cdot\mathbf{M}_2). \quad (7)$$

It is important to note that direct nuclear-nuclear interactions are excluded from this Hamiltonian. Each nuclear moment interacts only with the electrons of the same ion. Nevertheless, since the electronic spins are coupled together through the exchange interaction, the mechanism does permit an indirect nuclear-nuclear coupling. This is the Suhl-Nakamura interaction,[21,22] in which virtual magnons are excited and absorbed by two nuclei on the same sublattice. It is a consequence of the Suhl-Nakamura interaction that a well-defined nuclear spin-wave spectrum exists even though the nuclear polarization is of the order of 1%. deGennes et al.[27] have shown that the pullings of the nuclear resonant frequencies at low temperatures are also due to the Suhl-Nakamura interaction.

Finally, the equations of motion for the magnetization vectors are

$$\partial\mathbf{M}_i(t)/\partial t=-\Gamma\mathbf{M}_i\times(\partial\mathcal{3C}/\partial\mathbf{M}_i), \quad (8a)$$

$$\partial\mathbf{N}_i(t)/\partial t=-\gamma\mathbf{N}_i\times(\partial\mathcal{3C}/\partial\mathbf{N}_i). \quad (8b)$$

III. STATIC INTERACTION WITH APPLIED FIELD

In order to compute the numerical values of the normal mode frequencies, it is necessary to know the orientation of the magnetic sublattices as a function of applied field. Their positions may be obtained from the equation of motion, Eq. (8a), by setting the frequency to zero. In the steady state, the nuclear sublattices are always parallel to their respective electronic sublattices and exert no torque. Hence, Eq. (8b) need not be considered.

In the resonance analysis, we shall be primarily interested in the resonance spectrum when the magnetizing field $\mathbf{H}_0$ is applied along any of the three principal directions of the crystal—the $\langle 100\rangle$, $\langle 110\rangle$, or $\langle 111\rangle$ axes. For these particular configurations, the field and the magnetization lie in $\{110\}$ planes, and the static equilibrium problem can be solved using a two-dimensional model. The solution for a zero temperature approximation has been reported by Cole and Ince.[19,18] The complete three-dimensional analysis has been

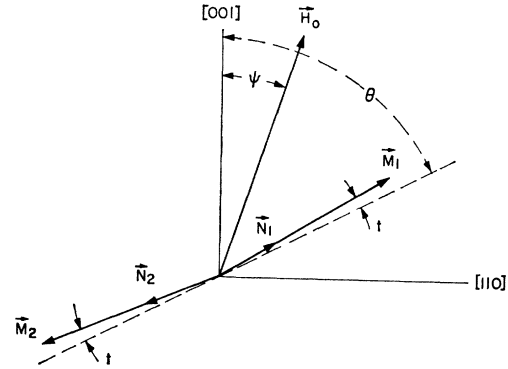[27] P. G. de Gennes et al., Phys. Rev. 129, 1105 (1963).

Fig. 1. Orientation of the electronic and nuclear sublattice magnetizations in the (110) plane. $\mathbf{H}_0$ lies in the same (110) plane.

performed by Platzker,[28] who also makes the approximation of zero temperature. In the following, the two-dimensional solution will be derived for arbitrary temperatures in the range $0\leq T<T_N$.

Figure 1 illustrates the magnetization vectors and the applied field in the (110) plane. $\mathbf{H}_0$ is applied in a direction making an angle ψ with the [001] axis. Under the action of the field, $\mathbf{M}_1$ and $\mathbf{M}_2$ rotate away from the [111] axis, which is the easy direction of magnetization. $\mathbf{M}_1$ and $\mathbf{M}_2$ also cant into the direction of the field, under the influence of the Zeeman torque, each by a small angle t which is given by

$$2M\sin t=\chi_\perp H_\perp, \quad (9)$$

M being the magnitude of $\mathbf{M}_1$ or $\mathbf{M}_2$ in zero field, $\chi_\perp$ is the perpendicular susceptibility, and $H_\perp$ is the resultant of $\mathbf{H}_0$ normal to the antiferromagnetic axis. The latter is represented by the dashed line in Fig. 1, and points at an angle θ with respect to the [001] axis.

For temperatures $T>0°K$, the simple relationship $|M_1|=|M_2|$ does not hold if $\mathbf{H}_0$ is applied at an arbitrary angle to the antiferromagnetic axis. To take account of this, the parallel susceptibility[29] $\chi_{||}$ is introduced. Then

$$M_1=M+\tfrac{1}{2}\chi_{||}H_{||}, \quad (10a)$$

$$M_2=-M+\tfrac{1}{2}\chi_{||}H_{||}, \quad (10b)$$

where $H_{||}$ is the resultant of $\mathbf{H}_0$ along the antiferromagnetic axis. Now consider the torques acting on $\mathbf{M}_1$ which must sum to zero for static equilibrium.

The Zeeman torque$=\mathbf{M}_1\times\mathbf{H}_0$

$$=-[M+\tfrac{1}{2}\chi_{||}H_{||}]\sin(\theta-\psi-t).$$

The exchange torque$=\mathbf{M}_1\times W_{12}\mathbf{M}_2$

$$=-|W_{12}|(M+\tfrac{1}{2}\chi_{||}H_{||})(M-\tfrac{1}{2}\chi_{||}H_{||})\sin 2t.$$

[28] A. Platzker, Ph.D. thesis proposal, M.I.T., 1968 (unpublished).
[29] T. Nagamiya et al., Advan. Phys. 4, 1 (1955).

Note that there is no term in the exchange torque involving W_{11}.

The anisotropy torque $= -\partial \mathcal{K}_a/\partial\theta$. Writing the components of $\mathbf{M_1}$ as functions of θ in Eq. (1) and performing the differentiation, we find

$$\partial \mathcal{K}_a/\partial\theta = \tfrac{1}{8}|K|[2\sin2(\theta-t)+3\sin4(\theta-t)].$$

Adding the torques and equating the sum to zero,

$$[M+\tfrac{1}{2}\chi_{11}H_0\cos(\theta-\psi-t)]H_0\sin(\theta-\psi-t)$$
$$-|W_{12}|[M^2-\tfrac{1}{4}(\chi_{11}{}^2H_0{}^2)\cos^2(\theta-\psi-t)]\sin2t$$
$$-\tfrac{1}{8}|K|[2\sin2(\theta-t)+3\sin4(\theta-t)]=0. \quad (11)$$

Similarly, for $\mathbf{M_2}$ the torque equation is

$$[M-\tfrac{1}{2}\chi_{11}H_0\cos(\theta-\psi+t)]H_0\sin(\theta-\psi+t)$$
$$-|W_{12}|[M^2-\tfrac{1}{4}(\chi^2{}_{11}H_0{}^2)\cos^2(\theta-\psi+t)]\sin2t$$
$$-\tfrac{1}{8}|K|[2\sin2(\theta+t)+3\sin4(\theta+t)]=0. \quad (12)$$

After making the approximations $\cos t \approx 1-2t^2$ and $\sin t \approx t$, Eqs. (11) and (12) are added to obtain

$$2t \approx H_0\sin(\theta-\psi)/|W_{12}|M. \quad (13)$$

Equations (9) and (13) are consistent provided $\chi_\perp = 1/|W_{12}|$. Subtracting Eq. (12) from Eq. (11) and substituting for t yields

$$H_0{}^2(1-\chi_{11}/\chi_\perp)\sin2(\theta-\psi) = -\tfrac{3}{4}H_EH_A\sin2\theta(1+3\cos2\theta)$$
$$+(\chi_{11}/\chi_\perp)^2(H_0{}^4/H_E{}^2)\sin2(\theta-\psi)\sin^2(\theta-\psi), \quad (14)$$

where $H_E = |W_{12}|M$ and $H_A = 4|K|/3M$. The second term on the right-hand side of Eq. (14) is small, and can be discarded. Finally,

$$H_0{}^2\sin2(\theta-\psi) = -[0.75H_EH_A/(1-\chi_{11}/\chi_\perp)]$$
$$\times\sin2\theta(1+3\cos2\theta). \quad (15)$$

Possible solutions of Eq. (15) will now be examined for the field directions of interest.

Case 1: H_0 parallel to the $[100]$ axis $(\psi=0)$

There are two possible solutions:

$$\text{(a)}\quad H_0{}^2 = -\frac{0.75H_EH_A}{(1-\chi_{11}/\chi_\perp)}(1+3\cos2\theta)$$

or

$$\text{(b)}\quad \sin2\theta=0.$$

Solution (a) is valid for the field range

$$0 \le H_0 \le \left[\frac{0.75H_EH_A}{1-\chi_{11}/\chi_\perp}\right]^{1/2},$$

over which θ varies between 54.7 and 90°. When H_0 is greater than

$$\left[\frac{0.75H_EH_A}{1-\chi_{11}/\chi_\perp}\right]^{1/2},$$

which is the spin-flopping value H_{sf}, solution (a) has no real solutions and solution (b) holds. For $H_0 > H_{sf}$, the minimum energy position of the magnetization corresponds to $\theta = 90°$. In the field range,

$$(0.75H_EH_A)^{1/2} \le H_0 \le \left[\frac{0.75H_EH_A}{1-\chi_{11}/\chi_\perp}\right]^{1/2},$$

both solutions are valid, since they both lead to real characteristic frequencies. For $H_0 < (0.75H_EH_A)^{1/2}$, solution (b) does not correspond to an energy minimum, and (a) is unique.

Case 2: H_0 parallel to the $[111]$ axis $(\psi=54.7°)$

Again, there are two possible solutions:

$$\text{(a)}\quad \theta=54.7°,$$

$$\text{(b)}\quad H_0{}^2 = -\frac{0.75H_EH_A}{(1-\chi_{11}/\chi_\perp)}\left(\frac{1+3\cos2\theta}{\sin2(\theta-\psi)}\right).$$

Solution (a) applies when H_0 is parallel to the antiferromagnetic axis. This configuration is always one of relative minimum energy. The absolute energy minimum corresponds to the range $125.3° \le \theta < 144.7°$ which is solution (b).

Case 3: H_0 parallel to the $[110]$ axis $(\psi=90°)$

Equation (15) yields only one solution:

$$H_0{}^2 = \frac{0.75H_EH_A}{(1-\chi_{11}/\chi_\perp)}\tan2\theta(1+3\cos2\theta).$$

The equivalent range of θ is

$$0° < \theta \le 54.7°.$$

This is a position of relative energy minimum. The direction of lowest energy, which is either $[\bar{1}11]$ or $[1\bar{1}1]$, is not predicted by Eq. (15). Both of these are easy axes, and the magnetization is flopped for any value of applied field.

IV. CHARACTERISTIC FREQUENCIES; TWO-SUBLATTICE MODEL

It has been demonstrated by earlier experiments that, in most respects, the AFMR frequencies for RbMnF$_3$ are well predicted by the two-sublattice model. The linearized equations of motion for the electronic sublattices which can be derived from Eq. (8a) are

$$j\omega\mathbf{m}_i/\Gamma = \mathbf{M}_i\times W_{12}\mathbf{m}_j+\mathbf{m}_i\times(\mathbf{H}_0+W_{12}\mathbf{M}_j+\alpha\mathbf{N}_i)+\delta\mathbf{T}_i$$
$$i, j=1, 2, \quad i\neq j. \quad (16)$$

Here, $\mathbf{M}_i$, $\mathbf{M}_j$, $\mathbf{N}_i$ are the static electronic and nuclear magnetization vectors, and $\mathbf{m}_i$, $\mathbf{m}_j$ are time-varying quantities. The tensor $\delta\mathbf{T}_i$ contains the terms resulting from the crystalline anisotropy.

The above equations, expressed in matrix form, become

$$j\omega \begin{bmatrix} \alpha_1 \\ \alpha_2 \end{bmatrix} = \begin{bmatrix} A_{11}+B_{11} & C_{12} \\ \cdots & \cdots \\ C_{21} & A_{22}+B_{22} \end{bmatrix} \begin{bmatrix} \alpha_1 \\ \alpha_2 \end{bmatrix}. \qquad (17)$$

α_1 and α_2 are column vectors, representing the rf components of the electronic sublattice magnetizations M_1 and M_2, referred to the crystal axes (ξ,η,ζ) along [100], [010], and [001], respectively. The matrices A_{11} and A_{22} contain the anisotropic components, while B and C matrices contain terms arising from the Zeeman, exchange, and hyperfine interactions. The superscript c indicates that the matrix components are referred to the crystal coordinates. These matrices are given in Ref. 19. Alternatively, they can be obtained from Appendix B by striking out the rows and columns corresponding to the RF components of the nuclear magnetization.

If we assume that the magnetization lies in the (110) plane, the number of equations contained in Eq. (17) can be reduced by transforming α_1 and α_2 to new coordinate systems, illustrated in Fig. 2. The appropriate transformations are expressed by

$$\begin{bmatrix} a_1 \\ a_2 \end{bmatrix} = \begin{bmatrix} R(-t)\cdot T & 0 \\ \cdots & \cdots \\ 0 & R(t)\cdot T \end{bmatrix} \begin{bmatrix} \alpha_1 \\ \alpha_2 \end{bmatrix}. \qquad (18)$$

The transformation T performs a twofold rotation. The first is through 45° about the [001] direction, the second is about the [1$\bar{1}$0] axis through the angle θ. In the new (x,y,z) coordinate system, the z direction is parallel to the antiferromagnetic axis, and the x axis lies in the (110) plane. The additional small rotation $R(-t)$ about the [$\bar{1}$10] axis transforms (x,y,z) into (x',y',z') with the z' axis parallel to M_1. Similarly, the additional rotation $R(t)$ about the [$\bar{1}$10] axis defines the third coordinate system (x'',y'',z''), with z'' parallel to $-M_2$. In the linearized theory, the rf components of sublattices 1 and 2 along the z' and z'' axes, respectively, are zero, and the set of equations in Eq. (17) is reduced from a set of six to a set of four. Hence,

$$\begin{bmatrix} A_{11}'+B_{11}'-j\omega I & C_{12}'\cdot R(-2t) \\ \cdots & \cdots \\ C_{21}''\cdot R(2t) & A_{22}''+B_{22}''-j\omega I \end{bmatrix} \begin{bmatrix} \alpha_1 \\ \alpha_2 \end{bmatrix} = 0. \qquad (19)$$

The superscript indicates the coordinate system to which the matrix components are referred.

The fourth-order characteristic equation is obtained by equating the determinant of the coefficient matrix to zero. In the zero temperature approximation $|M_1| = |M_2|$, and for this case Cole and Ince[19] deduced the following simple form for the characteristic equation:

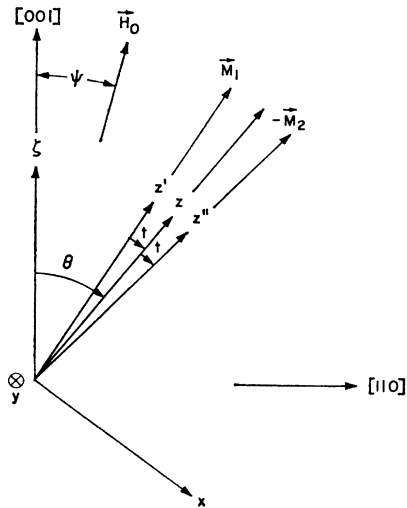$$(\omega^2-\Omega_+^2)(\omega^2-\Omega_-^2)-4(\Gamma H_0)^2\omega^2\cos^2(\theta-\psi)=0, \qquad (20)$$

FIG. 2. Illustration of transformed coordinate axes.

with

$$(\Omega_+/\Gamma)^2 \approx 2H_E(H_{NE}+a_{21})+H_0^2[2\sin^2(\theta-\psi)-1],$$

$$(\Omega_-/\Gamma)^2 \approx 2H_E(H_{NE}+a_{12})+H_0^2[\sin^2(\theta-\psi)-1],$$

and

$$a_{12}= -\tfrac{3}{2}H_A(1-\tfrac{7}{2}\sin^2\theta+\tfrac{3}{2}\sin^4\theta)=\tfrac{3}{2}H_A g(\theta), \qquad (21)$$

$$a_{21}= -\tfrac{3}{2}H_A[1-(13/2)\sin^2\theta+6\sin^4\theta]=\tfrac{3}{2}H_A f(\theta). \qquad (22)$$

Equation (20) has only two independent roots. The AFMR modes, with the field applied along the three principal axes, are illustrated in Figs. 3–7. The theo-
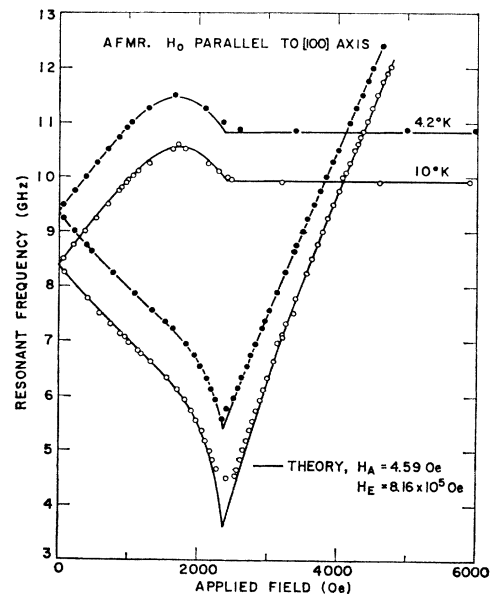

FIG. 3. AFMR modes in RbMnF$_3$. Resonant frequency versus applied field. The theoretical curves were obtained from the four-sublattice theory.

retical curves shown were actually derived from the four-sublattice model, but on the scale used in the figures, the small differences between the two theories do not show up.

When H_0 is applied in the [110] direction, the magnetization and the field are not in the same (110) plane. The frequencies are calculated by putting $(\theta-\psi)=90°$ in Eq. (20), and in Eqs. (21) and (22), θ is set equal to 54.7°.

Equation (20) is also valid for temperatures $T>0°K$ when M_1 and M_2 are flopped, since then the parallel susceptibility does not appear in the expressions for the resonant frequency. The resonant frequencies become

$$(\Omega_1/\Gamma)^2=(\Omega_+/\Gamma)^2\approx H_0^2+2H_E H_{NE}+3H_E H_A f(\theta) \quad (23)$$

and

$$(\Omega_2/\Gamma)^2=(\Omega_-/\Gamma)^2\approx 2H_E H_{NE}+3H_E H_A g(\theta). \quad (24)$$

The second mode is almost field-independent in the flopped configuration. The mode having the frequency Ω_1 is excited by applying a signal in the plane containing the antiferromagnetic axis. The mode with frequency Ω_2 is driven by applying the signal parallel to H_0. Hence, Ω_1 and Ω_2 are often referred to as the transverse and longitudinal modes, respectively.

Teaney et al.[2] were the first to study the flopped antiferromagnetic resonance modes in RbMnF$_3$. They considered directions of H_0 in the (100) plane as well as the (110) plane. Calculation of the resonant frequencies of the spin-flop modes is greatly simplified by knowing that the antiferromagnetic axis lies in the plane perpendicular to H_0. Also, it points in the direction of lowest anisotropy energy within this plane. For H_0 in the (100) plane, Teaney et al.[2,14] give the following expressions

for the AFMR frequencies:

$$(\Omega_1/\Gamma)^2\approx H_0^2+2H_E H_{NE}+3H_E H_A B(\theta_H,\varphi_H), \quad (25)$$

$$(\Omega_2/\Gamma)\approx 2H_E H_{NE}+3H_E H_A C(\theta_H,\varphi_H). \quad (26)$$

The angles θ_H and φ_H are the usual spherical coordinate angles of H_0, whereas in Eqs. (23) and (24) the angles refer to the antiferromagnetic axis. When H_0 is in the (100) plane,

$$B(\pi/2,\varphi_H)=-4 \cos4\varphi_H/(7+\cos4\varphi_H) \quad (27)$$

and

$$C(\pi/2,\varphi_H)=2(3+\cos4\varphi_H)/(7+\cos4\varphi_H). \quad (28)$$

If H_0 is in the (110) plane,

$$B\left(\theta_H,\frac{\pi}{4}\right)=-\left[1-\frac{13}{2}\cos^2\theta_H+6\cos^4\theta_H\right],$$
$$[001]\leq\theta_H<[111]; \quad (29)$$

$$=\frac{(2-\sin^2\theta_H)(3\sin^2\theta_H-1)}{(2+\sin^2\theta_H)},$$
$$[111]<\theta_H\leq[110]; \quad (30)$$

$$C\left(\theta_H,\frac{\pi}{4}\right)=\frac{3\cos^2\theta_H-1}{2(2-\cos^2\theta_H)}, \quad [001]\leq\theta_H<[111]; \quad (31)$$

$$=\frac{(1-3\cos^2\theta_H)(2-\cos^2\theta_H)}{(3-\cos^2\theta_H)},$$
$$[111]<\theta_H\leq[110]. \quad (32)$$

The equations of motion for the nuclear magnetization are

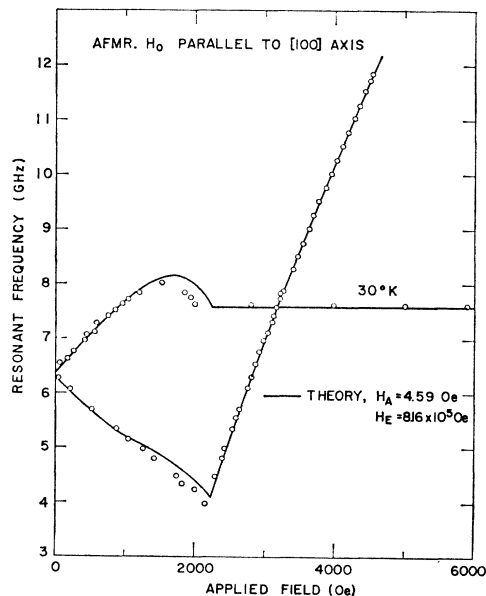$$j(\omega n_i/\gamma)=n_i\times(H_0+\alpha M_i)+\alpha N_i\times m_i, \quad i=1, 2. \quad (33)$$

FIG. 4. AFMR modes in RbMnF$_3$. Resonant frequency versus applied field at $T=30°K$. The theoretical curves were obtained from the four-sublattice theory.
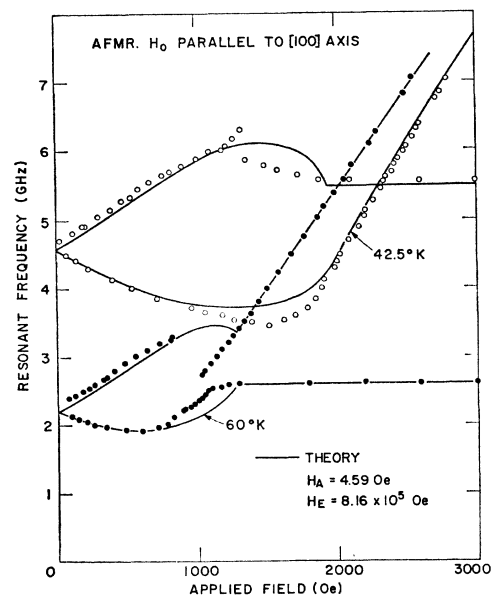

FIG. 5. AFMR modes in RbMnF$_3$. Resonant frequency versus applied field. The theoretical curves were obtained from the four-sublattice theory.
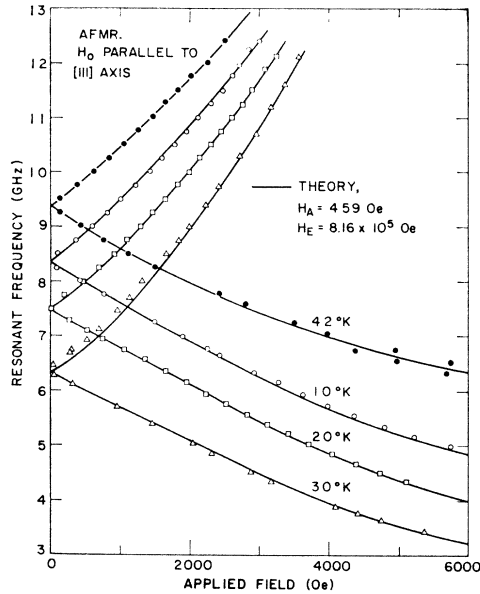
FIG. 6. AFMR modes in RbMnF$_3$. Resonant frequency versus applied field. The theoretical curves were obtained from the four-sublattice theory.
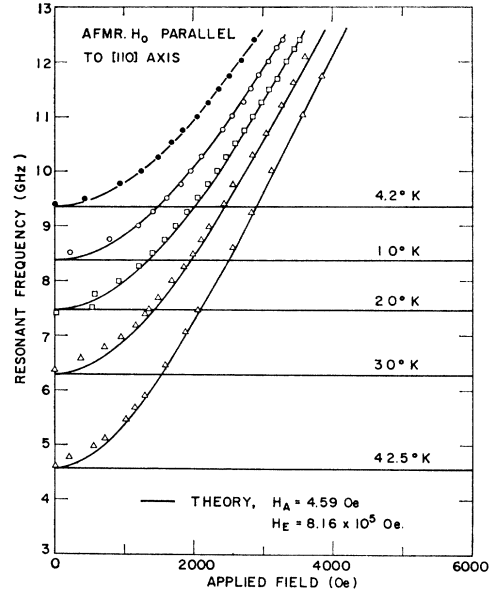

FIG. 7. AFMR modes in RbMnF$_3$. Resonant frequency versus applied field. The theoretical curves were obtained from the four-sublattice theory.

De Gennes et al.[27] have derived expressions for the nuclear resonant frequencies of a two-sublattice uniaxial antiferromagnet, with the magnetizing field applied parallel to the easy axis. They make the assumption that at the nuclear frequencies, the electronic spins respond adiabatically to the driving field, i.e., $\mathbf{M}_i$ is always parallel to $(\mathbf{H}_0 + \mathbf{H}_{A_i} + \alpha \mathbf{n}_i)$. The resonant frequencies at low temperatures are

$$\omega/\gamma = H_{NN}\left[1 - \frac{2\Gamma^2 H_E H_{NE}}{\Omega_1\Omega_2}\right]^{1/2}$$

$$\pm H_0\left[1 + \frac{\Gamma^2 H_{NE} H_{NN}}{\Omega_1\Omega_2}\right]. \quad (34)$$

For a canted antiferromagnet, the nuclear frequencies are given by

$$\left(\frac{\omega_{1,2}}{\gamma}\right) = H_{NN}\left[1 - \frac{2\Gamma^2 H_E H_{NE}}{\Omega^2_{1,2}}\right]^{1/2}. \quad (35)$$

Equation (35) predicts that one of the nuclear frequencies is independent of the applied field. This mode has not been detected experimentally in any material. The field tuneable flopped nuclear mode has been observed in several antiferromagnets, including RbMnF$_3$.[16] Equation (35) fits the measured data to within experimental error. It is not surprising that neither of the above equations yields the correct nuclear frequencies for RbMnF$_3$ when the magnetization is not flopped. The method of computing the NMR frequencies in small applied fields $(H < H_{sf})$, as well as for the spin-flow region will be discussed in Sec. V.

V. CHARACTERISTIC FREQUENCIES; FOUR-SUBLATTICE MODEL

The equations of motion for the electron and nuclear spins will now be solved simultaneously, taking into account the dynamic electron-nuclear correlation. As an adjunct to the theory, the temperature dependence of the relevant crystal parameters, based upon the molecular field approximation, has been included. Hence, the analysis also permits comparison with experimental results over a wide temperature range. The variation of the crystal parameters with temperature is discussed in Appendix A. The linearized equations of motion for the electronic spins are

$$j(\omega\mathbf{m}_i/\Gamma) = \mathbf{M}_i \times (W_{12}\mathbf{m}_j + \alpha\mathbf{n}_i) + \mathbf{m}_i$$
$$\times (\mathbf{H}_0 + W_{12}\mathbf{M}_j + \alpha\mathbf{N}_i) + \delta\mathbf{T}_i, \quad (36)$$

$$i,\ j = 1,\ 2 \quad i \neq j.$$

This differs from Eq. (16) by the addition of the rf nuclear magnetization. The equations of motion for the nuclear spins are still given by Eq. (33). Note that the crystalline anisotropy term does not enter into the nuclear equations and that there are no $\mathbf{n}_i \times \mathbf{n}_j$ terms. Written in the matrix form of Eq. (17), the rf magnetization vectors become

$$\alpha_i = \begin{bmatrix} m_{i\xi} \\ m_{i\eta} \\ m_{i\zeta} \\ n_{i\xi} \\ n_{i\eta} \\ n_{i\zeta} \end{bmatrix}. \quad (37)$$

The submatrices $A_{11}{}^c$, $B_{11}{}^c$, and $C_{12}{}^c$ are given in Appendix A. $A_{22}{}^c$, $B_{22}{}^c$, and $C_{21}{}^c$ are obtained from $A_{11}{}^c$, $B_{11}{}^c$, and $C_{12}{}^c$ by interchanging subscripts.

Transformations from the crystal coordinate axes to the (x',y',z') and (x'',y'',z'') systems of Fig. 2 are effected by the transformation matrices T and $R(t)$.

$$T = \begin{bmatrix} (\cos\theta)/\sqrt{2} & (\cos\theta)/\sqrt{2} & -\sin\theta & 0 & 0 & 0 \\ -1/\sqrt{2} & 1/\sqrt{2} & 0 & 0 & 0 & 0 \\ (\sin\theta)/\sqrt{2} & (\sin\theta)/\sqrt{2} & \cos\theta & 0 & 0 & 0 \\ 0 & 0 & 0 & (\cos\theta)/\sqrt{2} & (\cos\theta)/\sqrt{2} & -\sin\theta \\ 0 & 0 & 0 & -1/\sqrt{2} & 1/\sqrt{2} & 0 \\ 0 & 0 & 0 & (\sin\theta)/\sqrt{2} & (\sin\theta)/\sqrt{2} & \cos\theta \end{bmatrix}, \tag{38}$$

$$R(t) = \begin{bmatrix} \cos t & 0 & -\sin t & 0 & 0 & 0 \\ 0 & 1 & 0 & 0 & 0 & 0 \\ \sin t & 0 & \cos t & 0 & 0 & 0 \\ 0 & 0 & 0 & \cos t & 0 & -\sin t \\ 0 & 0 & 0 & 0 & 1 & 0 \\ 0 & 0 & 0 & \sin t & 0 & \cos t \end{bmatrix}. \tag{39}$$

The resonance matrix of Eq. (17) is reduced from 12×12 to 8×8 after the transformation by eliminating the z components of the rf magnetization, which are zero to first order. The component matrices become

$$B_{11}' = \begin{bmatrix} 0 & b_{12}' & 0 & -\Gamma \alpha M_1 \\ -b_{12}' & 0 & \Gamma \alpha M_1 & 0 \\ 0 & -\gamma \alpha N_1 & 0 & b_{34}' \\ \gamma \alpha N_1 & 0 & -b_{34}' & 0 \end{bmatrix}, \tag{40}$$

where

$$b_{12}' = \Gamma[H_0 \cos(\theta - \psi - t) + W_{12}M_2 \cos 2t + \alpha N_1]$$

and

$$b_{34}' = \gamma[H_0 \cos(\theta - \psi - t) + \alpha M_1].$$

$$B_{12}'R(-2t) = \Gamma \begin{bmatrix} 0 & -W_{12}M_1 & 0 & 0 \\ W_{12}M_1 \cos 2t & 0 & 0 & 0 \\ 0 & 0 & 0 & 0 \\ 0 & 0 & 0 & 0 \end{bmatrix}, \tag{41}$$

$$A_{11}' = \tfrac{3}{2}\Gamma H_A \cdot \begin{bmatrix} 0 & g(\theta) & 0 & 0 \\ -f(\theta) & 0 & 0 & 0 \\ 0 & 0 & 0 & 0 \\ 0 & 0 & 0 & 0 \end{bmatrix} \tag{42}$$

with

$$f(\theta) = -(1 - (13/2)\sin^2\theta + 6\sin^4\theta),$$

$$g(\theta) = -(1 - \tfrac{7}{2}\sin^2\theta + \tfrac{3}{2}\sin^4\theta).$$

The characteristic frequencies are the solutions of the equation

$$\left| \begin{bmatrix} A_{11}' + B_{11}' - j\omega I & \vdots & C_{12}'R(-2t) \\ \cdots\cdots\cdots\cdots & \vdots & \cdots\cdots\cdots\cdots \\ C_{21}''R(2t) & \vdots & A_{22}'' + B_{22}'' - j\omega I \end{bmatrix} \right| = 0$$

or

$$|[u - j\omega I]| = 0,$$

i.e.,

$$\left| \begin{bmatrix} -j\omega & u_{12} & 0 & u_{14} & 0 & u_{16} & 0 & 0 \\ u_{21} & -j\omega & u_{23} & 0 & u_{25} & 0 & 0 & 0 \\ 0 & u_{32} & -j\omega & u_{34} & 0 & 0 & 0 & 0 \\ u_{41} & 0 & u_{43} & -j\omega & 0 & 0 & 0 & 0 \\ 0 & u_{52} & 0 & 0 & -j\omega & u_{56} & 0 & u_{58} \\ u_{61} & 0 & 0 & 0 & u_{65} & -j\omega & u_{67} & 0 \\ 0 & 0 & 0 & 0 & 0 & u_{76} & -j\omega & u_{78} \\ 0 & 0 & 0 & 0 & u_{85} & 0 & u_{87} & -j\omega \end{bmatrix} \right| = 0. \tag{43}$$

The entries in the u matrix are written out in Appendix B. In order to simplify the determinant of Eq. (43), it is first rearranged.

$$\begin{vmatrix} \begin{bmatrix} u_{12} & u_{16} & u_{14} & 0 & \vdots & -j\omega & 0 & 0 & 0 \\ u_{52} & u_{56} & 0 & u_{58} & \vdots & 0 & -j\omega & 0 & 0 \\ u_{32} & 0 & u_{34} & 0 & \vdots & 0 & 0 & -j\omega & 0 \\ 0 & u_{76} & 0 & u_{78} & \vdots & 0 & 0 & 0 & -j\omega \\ \cdots & & & & \vdots & & & & \cdots \\ -j\omega & 0 & 0 & 0 & \vdots & u_{21} & u_{25} & u_{23} & 0 \\ 0 & -j\omega & 0 & 0 & \vdots & u_{61} & u_{65} & 0 & u_{67} \\ 0 & 0 & -j\omega & 0 & \vdots & u_{41} & 0 & u_{43} & 0 \\ 0 & 0 & 0 & -j\omega & \vdots & 0 & u_{85} & 0 & u_{87} \end{bmatrix} \end{vmatrix} = 0. \tag{44}$$

This equation is now equivalent to the equation

$$\begin{vmatrix} \begin{bmatrix} D_1 & \vdots & -j\omega I \\ \cdots & \vdots & \cdots \\ -j\omega I & \vdots & D_2 \end{bmatrix} \end{vmatrix} = 0,$$

which can be put in the form

$$|[\omega^2 I + D_1 D_2]| = 0.$$

At this point, further factorization is not possible if $H_0 < H_{sf}$, and the determinant must be multiplied out. The resulting characteristic equation is a fourth-order polynomial in ω^2. In general, none of the coefficients is zero, and the characteristic equation has to be solved by numerical methods.

Spin-Flop Frequencies

If the magnetization is flopped, considerable further simplification occurs as a consequence of the two conditions $|M_1| = |M_2|$ and $\cos(\theta - \psi) = 0$. It then follows that

$$A_{11}' = -A_{22}'' = A,$$
say,
$$B_{11}' = -B_2'' = B$$
and
$$C_{12}' \cdot R(2t) = -C_{21}'' \cdot R(-2t) = C,$$
i.e.,

$$\begin{vmatrix} \begin{bmatrix} A+B-j\omega I & \vdots & C \\ \cdots & \vdots & \cdots \\ -C & \vdots & -(A+B+j\omega I) \end{bmatrix} \end{vmatrix} = 0. \tag{45}$$

Instead of proceeding to the form Eq. (44), we pre- and post-multiply Eq. (45) by the matrix

$$\frac{1}{\sqrt{2}} \begin{bmatrix} I & \vdots & I \\ \cdots & \vdots & \cdots \\ I & \vdots & -I \end{bmatrix},$$

each identity submatrix being of rank 4. This step results in the equation

$$\begin{vmatrix} \begin{bmatrix} I & \vdots & (-1/j\omega)(A+B-C) \\ \cdots & \vdots & \cdots \\ -(1/j\omega)(A+B+C) & \vdots & I \end{bmatrix} \end{vmatrix} = 0$$

and hence,

$$|[\omega^2 I + (A+B+C)(A+B-C)]| = 0. \tag{46}$$

In this manner, a reduction from an 8×8 to a 4×4

determinantal equation [Eq. (46)] has been made. The utility of Eq. (46) is that the nonzero entries in the matrix are arranged in a checkerboard manner, and therefore can be factorized by inspection. It should be emphasized that this method of reduction does not work if $H_0 < H_{sf}$.

A pair of biquadratic equations is obtained. Each one contains one electronic and one nuclear resonant frequency. After insignificant terms have been discarded, these equations are

$$\omega^4 - \omega^2(\Omega_{i0}^2 + 2\Omega_{NE}^2 + \omega_N^2) + \Omega_{i0}^2 \omega_N^2 \approx 0, \quad i=1, 2 \tag{47}$$

where $\Omega_{NE}^2 = 2\Gamma^2 H_E H_{NE}$. The terms Ω_{10}^2, Ω_{20}^2 represent the AFMR frequencies, with the coupling coefficient α set to zero, i.e.,

$$(\Omega_{10}/\Gamma)^2 = H_0^2 + 3H_E H_A f(\theta), \tag{48}$$

$$(\Omega_{20}/\Gamma)^2 = 3H_E H_A g(\theta). \tag{49}$$

Equation (47) was first derived by Turov and Kuleev.[30]

The resonant frequencies will be calculated with the approximation

$$(\Omega_{i0}^2 + 2\Omega_{NE}^2 + \omega_N^2) \approx \Omega_{i0}\omega_N. \tag{50}$$

Since (Ω_{i0}/ω_N) can be less than unity in very low anisotropy antiferromagnets (e.g., CsMnF$_3$) we require Eq. (50) to imply that $\Omega_{NE}^2 \gg \Omega_{i0}\omega_N$, i.e., there is strong electron-nuclear correlation. The roots of Eq. (47) are

$$\omega^2 = \tfrac{1}{2}(\Omega_{i0}^2 + 2\Omega_{NE}^2 + \omega_N^2) \pm \tfrac{1}{2}[(\Omega_{i0}^2 + 2\Omega_{NE}^2 + \omega_N^2)^2 - 4\Omega_{i0}^2\omega_N^2]^{1/2}. \tag{51}$$

Hence,

$$\omega^2 = \Omega_i^2 \approx \Omega_{i0}^2 + 2\Omega_{NE}^2 + \omega_N^2, \quad i=1, 2 \tag{52}$$

and

$$\omega_i^2 \approx \frac{\Omega_{i0}^2\omega_N^2}{\Omega_{i0}^2 + 2\Omega_{NE}^2 + \omega_N^2} = \omega_N^2 \left[1 - \frac{(2\Omega_{NE}^2 + \omega_N^2)}{\Omega_i^2}\right]. \tag{53}$$

At this point, a comparison between the two- and four-sublattice theories can be made. Equation (52) differs from Eqs. (23) and (24) by the term ω_N^2. Hence, compared to the two-sublattice theory, the four-sublattice

[30] E. A. Turov and V. G. Kuleev, Zh. Eksperim. i Teor. Fiz. **49**, 248 (1965) [English transl.: Soviet Phys.—JETP **22**, 176 (1966)].
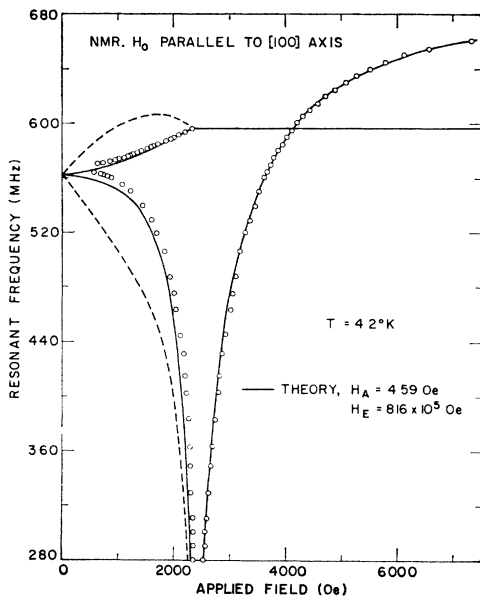
FIG. 8. NMR modes in RbMnF$_3$ at $T = 4.2°K$. Mn[55] resonant frequency versus applied field. The solid lines represent the four-sublattice theory. The dashed lines were derived from Eq. (35), due to de Gennes *et al.* (Ref. 27).

approach raises the AFMR frequencies by approximately $\omega_N^2/2\Omega_i$, which is about 50 MHz in the low-temperature approximation. This shift is less than the linewidth (~ 250 MHz) and would not be detectable. Comparing Eq. (35) with Eq. (53), it is seen that the nuclear frequencies calculated from the four-sublattice model are lower. The shift is roughly equal to $\frac{1}{2}\omega_i(\omega_N/\Omega_i)^2$, or a maximum of about 4 MHz, which is larger than the linewidth. Freiser *et al.*[16] report the half-linewidth for the flopped nuclear mode to be 0.28 MHz.
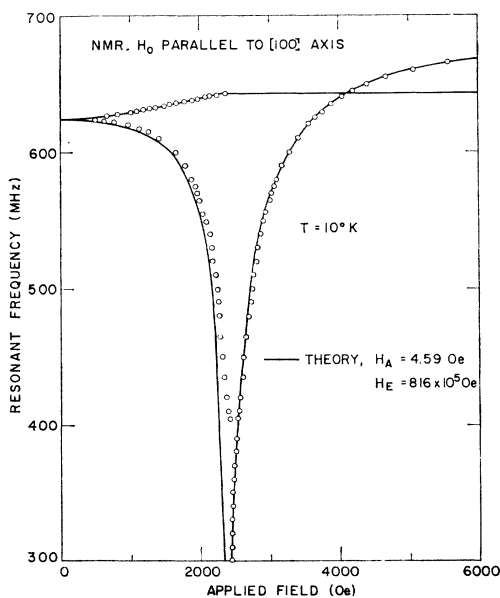

FIG. 9. NMR modes in RbMnF$_3$ at $T = 10°K$. Mn[55] resonant frequency versus applied field. The theoretical curves were derived from the four-sublattice theory.

VI. EXPERIMENTS

The experimental arrangement for studying coupled AFMR-NMR in RbMnF$_3$ was designed to permit measurements to be made over a very wide frequency range, and at temperatures within the bounds $4.2°K \leq T < T_N$. The AFMR data covered a frequency span of 1–12.5 GHz, while NMR measurements extended over the range 250–687 MHz. The two frequency bands were covered using three cavities, two waveguide and one coaxial type. The rectangular waveguide versions, which were used between the frequency limits 3.6 and 12.5 GHz, operated in the TE_{10n} modes. Both cavities could be tuned with shorting plungers external to the Dewar vessel. The coupling probe was also located outside the Dewar, at room temperature, so that the coupling could be optimized for maximum sensitivity at each frequency.

The cavities were constructed from stainless steel, except for a copper end section which contained the sample. The latter was mounted on the end wall of the waveguide, using double-sided adhesive tape. RbMnF$_3$ is a soft material, and other adhesives commonly used for mounting specimens, such as cryogenic varnish, would fracture the crystal on cooling. In order to remove the sample, the tape was dissolved off with ethyl acetate, which caused no apparent damage to the sample.

The sample orientation with respect to the steady field could be changed by rotating the entire waveguide assembly and Dewar vessel. This avoided the need for gears within the Dewar. Unfortunately, since the angle between the rf field and the steady field changed with the rotation, the rf coupling to the sample also varied.

The rf signal reflected from the cavity was detected and amplified using a high-gain differential amplifier with a dc offset. When the signal source was operated in a stabilized cw mode, the sample resonance was located using magnetic field sweep and a pen recorder display. Alternatively, the source could be frequency-modulated, and the output from the differential amplifier displayed on an oscilloscope. These detection schemes provided adequate sensitivity for investigating NMR as well as AFMR. In the NMR work, magnetic field modulation with phase sensitive detection was tried. In order to eliminate the skin depth problem, the modulating coil was placed inside the rf cavity. The maximum modulation amplitude that was available was less than 1 Oe, and the sensitivity achieved was no better than with dc detection. For measurement of the applied field for resonance, a rotating coil fluxmeter, calibrated to an accuracy of 0.1 Oe, was used.

The coaxial cavity was employed at low microwave frequencies and in the NMR frequency band. It was externally tuneable, employed loop coupling, and operated in the TEM mode.

The sample temperature was varied by a servo-controlled heater coil, which was wound onto the cavity end section. In the temperature range 4.2–40°K, a
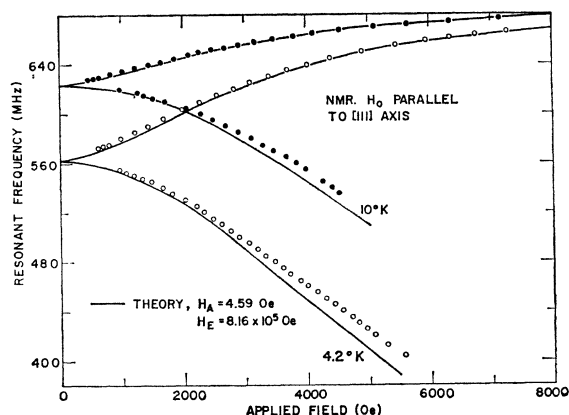
FIG. 10. NMR modes in RbMnF$_3$. Mn[55] resonant frequency versus applied field. The theoretical curves were derived from the four-sublattice theory.

FIG. 11. NMR modes in RbMnF$_3$. Mn[55] resonant frequency versus applied field. The theoretical curves were derived from the four-sublattice theory.

germanium resistance thermometer was used as the sensing element. At higher temperatures, a platinum resistance thermometer proved to be more sensitive. The temperature of the sensor could be stabilized to better than $\pm 0.1°$K. The sensor was embedded in the cavity wall and was located about $\frac{1}{8}$ in. from the sample. Any uncertainty in the sample temperature would be due chiefly to (1) the temperature gradient across the sample adhesive, and (2) the sample size.

Experimental data for the AFMR modes are shown in Figs. 3–7. The solid lines are the theoretical results obtained from the four-sublattice model. Several different samples were used in the experimental work, in order to check that the resonance characteristics were consistent. With the magnetizing field applied in the [111] or [110] direction, only those resonances corresponding to the direction of the magnetization having the lowest energy were detected. The AFMR modes were examined at temperatures up to 70°K. Since there were no provisions for pumping on the liquid helium, measurements were not extended below 4.2°K.

The NMR measurements are illustrated in Figs. 8–12. Data were taken over the temperature range 4.2–30°K. The solid lines represent frequencies obtained from the four-sublattice coupled mode theory. The dashed line in Fig. 8. represents the NMR frequencies calculated from the de Gennes pulling formula.[27] Above spin-flop, the frequencies obtained from the two theories are almost indistinguishable.

RbMnF$_3$ samples were cut from single crystals grown by the Czochralski method.[31] The sample shape was cubic, of side 5 mm, two faces being $\langle 100 \rangle$ planes and the remainder $\langle 110 \rangle$ planes. This size was suitable for both AFMR and NMR experiments. The data shown in Figs. 3–12 were all taken with one specimen. Sample shape was considered unimportant, since demagnetizing and cavity wall effects were insignificant.

[31] P. O. Henk et al., Department of Electrical Engineering and Center for Materials Science and Engineering, M.I.T. Technical Memo No. 3., 1966 (unpublished).
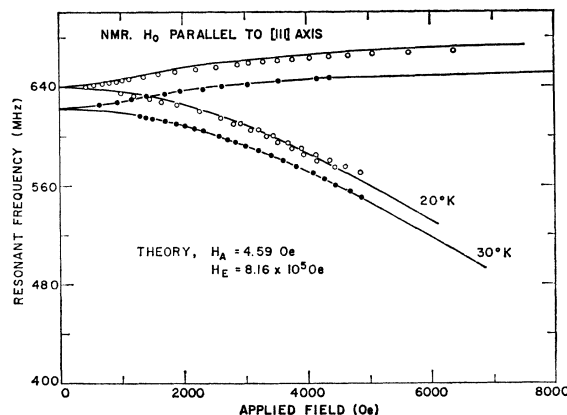
VII. DISCUSSION OF RESULTS

First of all, comparison will be made between theory and experiment for low temperatures, say 10°K or less, where the parallel susceptibility can be ignored. At the AFMR frequencies, the agreement is very good. In order to get the best possible fit between the theoretical curves and the experimental points, accurate values of H_{NE}, H_E, and H_A are crucial. The value of H_{NE} was taken from the work of Freiser et al.[16] H_E and H_A were found by measuring the field for spin-flop resonance for two different crystal orientations. From Eq. (52) the $H_E H_A$ product is

$$\tfrac{7}{2} H_E H_A = H_{0[100]}{}^2 - H_{0[110]}{}^2. \qquad (54)$$

Substituting for $H_E H_A$ in Eqs. (52), and neglecting ω_N, yields H_A and H_E separately. A further check is provided by the zero-field frequency. The anisotropy field was found to be 4.59 Oe at 4.2°K. The value of H_E adopted, 8.16×10^5 Oe, is significantly lower than the value reported by Teaney et al.[2] The new measurement should have less uncertainty, since at X-band
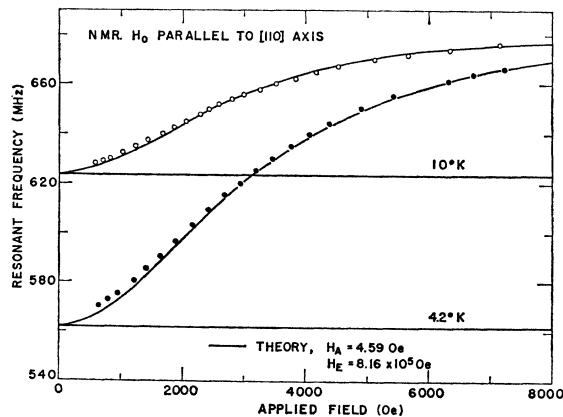

FIG. 12. NMR modes in RbMnF$_3$. Mn[55] resonant frequency versus applied field. The theoretical curves were derived from the four-sublattice theory.
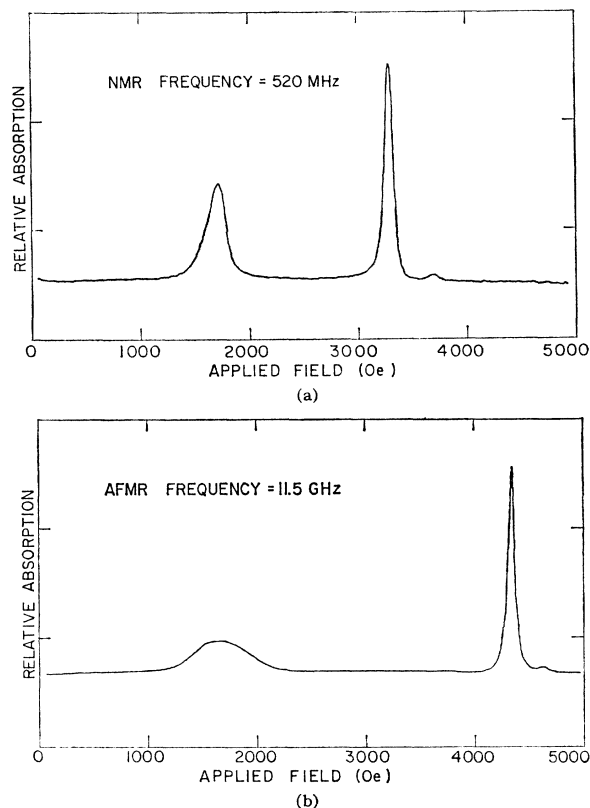
Fig. 13. (a) NMR in RbMnF₃. Cavity absorption versus applied field at 520 MHz; (b) AFMR in RbMnF₃. Cavity absorption versus applied field at 11.5 GHz.

frequencies, the field for resonance is much smaller than at the frequency of 23 GHz, used by Teaney *et al.*

Two additional parameters required for computing the nuclear frequencies are the internal nuclear field H_{NN} and the hyperfine frequency. H_{NN} was assumed[15] to be 6.54×10^5 Oe; $\omega_N(=686.2$ MHz) was taken from previous NMR measurements.[15] The latter value is consistent with that obtained from double-resonance experiments.[32] The fit between the theoretical and experimental NMR modes is not quite as good as for AFMR. The discrepancy is worst near zero field. The fit could probably be improved by parameter adjustment. There is also a pronounced deviation when the field is applied in the [111] direction, only part of which can be attributed to crystal misalignment.

Both nuclear modes are detectable if H_0 is in the [111] or [100] directions. For the [100] configuration (Fig. 8) the spectrum is particularly interesting. The modes could be followed over more than an octave range of frequency, from 250 to about 660 MHz. The upper frequency limit was set by the available bias field (≈ 7000 Oe). At the lower frequencies, the fields for resonance of the two modes are close together. At 250 MHz, the modes merged into a single broad resonance.

The NMR linewidth of the flopped mode is about 100 Oe, as illustrated by Fig. 13(a). The AFMR line-

³² W. J. Ince, J. Appl. Phys. 40, 1595 (1969).

width, for this particular sample, is comparable. Figure 13(b) shows the relative cavity absorption versus applied field at the AFMR frequency of 11.5 GHz. Below spin-flop, the line shape is affected by the change in sublattice orientation with applied field.

In addition to the low field and flopped resonance lines predicted by the theory, Fig. 13(a) shows a third small peak. It is located at a field strength of about 3700 Oe close to the flopped resonance line. A similar satellite line is apparent at the AFMR frequency, and may be attributed to domain effects. When H_0 is parallel to the [001] axis, the magnetization may be flopped along either the [110] or [1̄10] axes, which are equivalent in free energy. A small misalignment of the crystal will remove the degeneracy.

A comparison of the two- and four-sublattice theories has shown that they lead to almost the same values for the AFMR frequencies, the differences being entirely negligible. In the case of the field tuneable NMR mode, the de Gennes pulling formula predicts a resonant frequency that is slightly higher (~ 4 MHz) than the value derived from the four-sublattice model. Unfortunately, the shift is probably too small to be detected, being smaller than the experimental errors introduced by crystal misalignment and uncertainties in crystal parameter values. However, the four-sublattice analysis has permitted solution of the NMR modes below spin-flop, where the de Gennes formula [Eq. (35)], is clearly inapplicable. The agreement between theory and experiment in this range of applied field is considered good.

The AFMR modes were investigated at roughly 10° temperature intervals in the range 4.2–70°K. A sampling of the results is shown in Figs. 3–7. With the magnetizing applied in the [110] or [111] directions, the variation of frequency with temperature is well predicted by the theory, if the temperature dependence of the crystal parameters (as discussed in Appendix A) is included.

With the field parallel to the [100] axis, the agreement is less convincing, particularly at temperatures in excess of 40°K. According to theory, as the temperature is raised, the intersection of the two flopped AFMR modes occurs at a gradually decreasing value of applied field. Eventually, the crossover field coincides with the spin-flop field. The two resonant frequencies are given by the expressions

$$(\Omega_1/\Gamma)_{[100]}^2 \approx H_0^2 + 2H_E H_{NE} - \tfrac{3}{2} H_E H_A, \quad (55)$$

$$(\Omega_2/\Gamma)_{[100]}^2 \approx 2H_E H_{NE} + 3H_E H_A. \quad (56)$$

It follows that $\Omega_1 = \Omega_2$ when $H_0^2 = (9/2)H_E H_A$. Hence, the crossover and spin-flop coincide if

$$H_{sf}^2 = 1.5 H_E H_A / (1 - \chi_{11}/\chi_\perp) = \tfrac{9}{2} H_E H_A,$$

which is satisfied when $\chi_{11}/\chi_\perp = \tfrac{2}{3}$. Applying formula (A4), it is estimated that this condition should be met at about 50°K. At higher temperatures there will be no intersection, as illustrated by the mode plot for 60°K in Fig. 5.

According to Sec. III, when the applied field is parallel to the [100] axis, the flopped configuration is still a position of minimum energy for field strengths down to $(\frac{3}{2}H_E H_A)^{1/2}$ Oe. Hence, in the field range $(\frac{3}{2}H_E H_A)^{1/2} < H_0 < H_{sf}$, one expects the mode pattern to be more complicated, because there are two possible directions for the magnetization in the (110) plane. Another factor to be considered is crystal misalignment, which causes a mixing of the two flopped AFMR modes and a splitting in the crossover region. Even a small misalignment of say 1° which has only a small effect at 4.2°K, produces a pronounced splitting at higher temperatures.

Experimentally, the low-field resonances were very weak at temperatures greater than 50°K. Consider, for example, the experimental data shown in Fig. 5, corresponding to 60°K. The resonances at fields less than 1200 Oe were just detectable. The rising mode branch in the low-field region became progressively weaker, and could not be followed at fields greater than about 800 Oe. It is not clear where the two segments of the upper mode branch finally connect.

The NMR modes were investigated at temperatures up to 30°K. As in the case of the AFMR modes, the agreement between theory and experiment was excellent if the field was applied in the [110] or [111] directions, but was poorer for the [100] resonances.

ACKNOWLEDGMENTS

APPENDIX A: TEMPERATURE DEPENDENCE OF CRYSTAL PARAMETERS

In order to compute the normal mode frequencies as a function of temperature, M_1 and M_2 are assumed to obey the $S = \frac{5}{2}$ Brillouin function. The parallel susceptibility is then given by the formula[33]

$$\chi_{11}(T) = \frac{N g_E^2 \mu_E^2 S^2 B_{5/2}'(a)}{kT - \frac{1}{2}(N^2 g_E^2 \mu_E^2 S^2)(W_{11} + W_{12}) B_{5/2}'(a)}, \quad (A1)$$

with

$$a = (g_E \mu_E S / kT)(W_{11} M_1 + W_{12} M_2).$$

N is the number of ions per unit volume and W_{11} and W_{12} are the exchange constants. It is more convenient to express χ_{11} in normalized form. This is done by making use of the following standard expressions for

[33] A. H. Morrish, *The Physical Principles of Magnetism* (Wiley-Interscience, Inc., New York, 1965), p. 451.
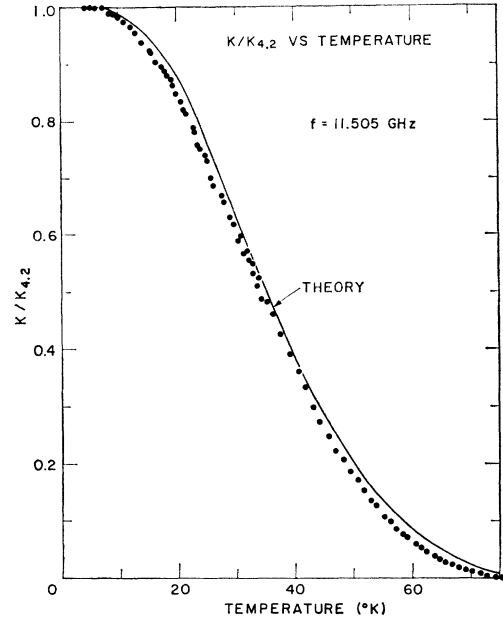

FIG. 14. Variation of the cubic anisotropy constant K with temperature. The theoretical curve is based on a single ion model (Ref. 34).

the Néel temperature T_N and the negative temperature intercept T_θ of the Néel theory.[33]

$$T_N = \frac{N g_E^2 \mu_E^2 S(S+1)}{6k}(W_{11} - W_{12}), \quad (A2)$$

$$T_\theta = \frac{N g_E^2 \mu_E^2 S(S+1)}{6k}(W_{11} + W_{12}). \quad (A3)$$

Hence,

$$\left(\frac{\chi_{11}}{\chi_\perp}\right)_T = \frac{(15/7)(T_N - T_\theta)B_{5/2}'(a)}{T - (15/7)T_\theta B_{5/2}'(a)}. \quad (A4)$$

T_N and T_θ are taken to be 82.6 and $-160°K$, respectively.[16,17] M_1 and M_2 can be written as

$$M_{1,2} = \pm(M \pm \frac{1}{2}\chi_{11}H_{11}) = \pm M_0 B_{5/2}(a)$$
$$\times[1 \pm (\chi_{11}/\chi_\perp)(H_{11}/2H_E)],$$

where $H_E = B_{5/2}(a)H_E(T=0)$. It has been tacitly assumed that W_{12} is temperature-insensitive.

The nuclear hyperfine fields can also be related to the Brillouin function, since

$$H_{NN} = \alpha M_{1,2} = H_{NN}(T=0)(M_{1,2}/M_0),$$

and from Eq. (5)

$$H_{NE} \approx (A^2/\Gamma h)[I(I+1)/3kT]SB_{5/2}(a)$$
$$= (9.43/T)B_{5/2}(a).$$

The small temperature dependence of the hyperfine interaction constant is ignored here.

The crystalline anisotropy constant, normalized to its zero-degree value may be written as a function of

the $H_E H_A$ product:

$$K/K_0 = H_E H_A / (H_E H_A)_0.$$

The latter can be obtained from antiferromagnetic resonance [see Eq. (54)]. Figure 14 shows the measured dependence of $K/K_{4.2}(\approx K/K_0)$ versus temperature, taken at the AFMR frequency of 11.505 GHz. The solid line shows the calculated variation, based on the Wolf single ion theory.[16,34]

APPENDIX B: DETAILS OF RESONANCE ANALYSIS

In the crystal axis system of coordinates (ξ,η,ζ) the equations of motion for the four-sublattice model

are

$$j\omega\begin{bmatrix}\alpha_1\\\alpha_2\end{bmatrix}=\begin{bmatrix}A_{11}+B_{11} & C_{12}\\C_{21} & A_{22}+B_{22}\end{bmatrix}^c\begin{bmatrix}\alpha_1\\\alpha_2\end{bmatrix}. \quad (B1)$$

The column vectors α_1, α_2 represent the rf components of the magnetization.

$$\alpha_i=\begin{bmatrix}m_{i\xi}\\m_{i\eta}\\m_{i\zeta}\\n_{i\xi}\\n_{i\eta}\\n_{i\zeta}\end{bmatrix}. \quad (B2)$$

The coefficient matrix is partitioned into 6×6 submatrices. $A_{11}{}^c$ is the anisotropy array referred to the crystal axis system.

$$A_{11}{}^c=\tfrac{3}{2}(\Gamma H_A/M^3)\begin{bmatrix}0 & (3M_{1\zeta}M_{1\eta}{}^2-M_{1\zeta}{}^3) & -(3M_{1\eta}M_{1\zeta}{}^2-M_{1\eta}{}^3) & 0 & 0 & 0\\-(3M_{1\zeta}M_{1\xi}{}^2-M_{1\zeta}{}^3) & 0 & (3M_{1\xi}M_{1\zeta}{}^2-M_{1\xi}{}^3) & 0 & 0 & 0\\(3M_{1\eta}M_{1\xi}{}^2-M_{1\eta}{}^3) & -(3M_{1\xi}M_{1\eta}{}^2-M_{1\xi}{}^3) & 0 & 0 & 0 & 0\\0 & 0 & 0 & 0 & 0 & 0\\0 & 0 & 0 & 0 & 0 & 0\\0 & 0 & 0 & 0 & 0 & 0\end{bmatrix}.$$

The submatrix $B_{11}{}^c$ contains Zeeman, exchange, and hyperfine interaction terms:

$$B_{11}{}^c=\begin{bmatrix}0 & b_{12}{}^c & b_{13}{}^c & 0 & -\Gamma\alpha M_{1\zeta} & \Gamma\alpha M_{1\eta}\\-b_{12}{}^c & 0 & b_{23}{}^c & \Gamma\alpha M_{1\zeta} & 0 & -\Gamma\alpha M_{1\xi}\\-b_{13}{}^c & -b_{23}{}^c & 0 & -\Gamma\alpha M_{1\eta} & \Gamma\alpha M_{1\xi} & 0\\0 & -\gamma\alpha N_{1\zeta} & \gamma\alpha N_{1\eta} & 0 & \gamma(H_{0\zeta}+\alpha M_{1\zeta}) & -\gamma(H_{0\eta}+\alpha M_{1\eta})\\\gamma\alpha N_{1\zeta} & 0 & -\gamma\alpha N_{1\xi} & -\gamma(H_{0\zeta}+\alpha M_{1\zeta}) & 0 & \gamma(H_{0\xi}+\alpha M_{1\xi})\\-\gamma\alpha N_{1\eta} & \gamma\alpha N_{1\xi} & 0 & \gamma(H_{0\eta}+\alpha M_{1\eta}) & -\gamma(H_{0\xi}+\alpha M_{1\xi}) & 0\end{bmatrix},$$

where

$$b_{12}{}^c=\Gamma(H_{0\zeta}+W_{12}M_{2\zeta}+\alpha N_{1\zeta}),$$

$$b_{13}{}^c=-\Gamma(H_{0\eta}+W_{12}M_{2\eta}+\alpha N_{1\eta}),$$

$$b_{23}{}^c=\Gamma(H_{0\xi}+W_{12}M_{2\xi}+\alpha N_{1\xi}).$$

$C_{12}{}^c$ contains exchange terms:

$$C_{12}{}^c=\Gamma\begin{bmatrix}0 & -W_{12}M_{1\zeta} & W_{12}M_{1\eta} & 0 & 0 & 0\\W_{12}M_{1\zeta} & 0 & -W_{12}M_{1\xi} & 0 & 0 & 0\\-W_{12}M_{1\eta} & W_{12}M_{1\xi} & 0 & 0 & 0 & 0\\0 & 0 & 0 & 0 & 0 & 0\\0 & 0 & 0 & 0 & 0 & 0\\0 & 0 & 0 & 0 & 0 & 0\end{bmatrix}.$$

The submatrices $A_{22}{}^c$, $B_{22}{}^c$, and $C_{21}{}^c$ can be derived from $A_{11}{}^c$, $B_{11}{}^c$, and $C_{12}{}^c$, by interchanging suffixes 1 and 2.

After applying the transformations of Eq. (18), i.e.,

$$a_1=R(-t)T\alpha_1,$$

$$a=R(t)T\alpha_2,$$

the characteristic equation is obtained from the condition

$$[u-j\omega I]=0. \quad (B3)$$

In Eq. (B3), u is the transformed 8×8 coefficient matrix, whose nonzero entries are as follows:

$$u_{12}=\Gamma[H_0\cos(\theta-\psi-t)+W_{12}M_2\cos2t+\alpha N_1+\tfrac{3}{2}H_A g(\theta)],$$

$$u_{14}=-u_{23}=-\Gamma\alpha M_1,$$

$$u_{16}=-\Gamma W_{12}M_1,$$

$$u_{21}=-\Gamma[H_0\cos(\theta-\psi-t)+W_{12}M_2\cos2t+\alpha N_1+\tfrac{3}{2}H_A f(\theta)],$$

$$u_{25}=\Gamma W_{12}M_1\cos2t,$$

$$u_{32}=-u_{41}=-\gamma\alpha N_1,$$

$$u_{34}=-u_{43}=\gamma[H_0\cos(\theta-\psi-t)+\alpha M_1],$$

$$u_{52}=-\Gamma W_{12}M_2,$$

$$u_{56}=\Gamma[H_0\cos(\theta-\psi+t)+W_{12}M_1\cos2t+\alpha N_2-\tfrac{3}{2}H_A g(\theta)],$$

$$u_{58}=-u_{67}=-\Gamma\alpha M_2,$$

$$u_{61}=\Gamma W_{12}M_2\cos2t,$$

$$u_{65}=-\Gamma[H_0\cos(\theta-\psi+t)+W_{12}M_1\cos2t+\alpha N_2-\tfrac{3}{2}H_A f(\theta)],$$

$$u_{76}=-u_{85}=-\gamma\alpha N_2,$$

$$u_{78}=-u_{87}=\gamma[H_0\cos(\theta-\psi+t)+\alpha M_2].$$

[34] W. P. Wolf, Phys. Rev. **108**, 1152 (1957).